

On the breakup of a thin liquid film subject to interfacial shear

By HAMED H. SABER AND MOHAMED S. EL-GENK†

Institute for Space and Nuclear Power Studies and Chemical and Nuclear Engineering Department,
University of New Mexico, Albuquerque, NM 87131, USA

(Received 28 June 2002 and in revised form 25 August 2003)

The breakup of a thin non-evaporating liquid film that is either flowing down or climbing on a vertical or inclined surface and subject to cocurrent or countercurrent interfacial shear (or gas flow) is investigated analytically. Analytical expressions for the dimensionless liquid film thickness, Δ_{min} , and wetting rate, Γ_{min} , at breakup are derived based on the minimization of the total energy of a stable rivulet, formed following the film breakup. For a downflowing liquid film, increasing the cocurrent interfacial shear (or gas velocity) or decreasing the equilibrium contact angle, θ_o , decreases both Δ_{min} and Γ_{min} , below their values with zero interfacial shear. Conversely, increasing the countercurrent interfacial shear or θ_o , increases both Δ_{min} and Γ_{min} , above their values with zero interfacial shear. The predictions of Δ_{min} and Γ_{min} for a climbing water film on a vertical surface are in good agreement with reported experimental data for a wide range of cocurrent gas velocities.

1. Introduction

The breakup of a downflowing or a climbing thin liquid film on a vertical or an inclined surface, subject to either cocurrent or countercurrent interfacial shear or gas flow, is of interest in many industrial applications and processes (Hartely & Murgatroyd 1964; Hobler 1964; Hewitt & Lacey 1965; Ponter *et al.* 1967; Bankoff 1971; Munakata, Watanabe & Miyashita 1975; Mikielewicz & Moszynski 1976; Andros 1980; Doniec 1991; El-Genk & Saber 2001, 2002). Examples include distillation, closed two-phase thermosyphons, wetted columns, cooling towers, thin-film heat exchangers, painting, and cooling of nuclear fuel rods following the accidental loss of coolant in a light water reactor (LWR). Some of these applications are concerned with the breakup of evaporating thin liquid films, which has been addressed in a prior publication (El-Genk & Saber 2002). The focus of this paper is on the breakup of a non-evaporating liquid film that is subject to a cocurrent or countercurrent interfacial shear or gas velocity.

The breakup of a thin liquid film flowing down a vertical or inclined surface and the stability of the resulting rivulets is a complex dynamic process (Young & Davis 1987; King & Tuck 1993; Kalliadasis 2002; Wilson, Duffy & Hunt 2002). Under certain conditions, the breakup of the liquid film results in the formation of stable parallel rivulets separated by dry patches (figure 1), which is the basis for the present study. Such rivulets have been observed experimentally (Ponter *et al.* 1967; Munakata *et al.* 1975; and Andros 1980) (figure 1*a*). The height of such a stable rivulet at the plane

† Author to whom correspondence should be addressed: mgenk@unm.edu

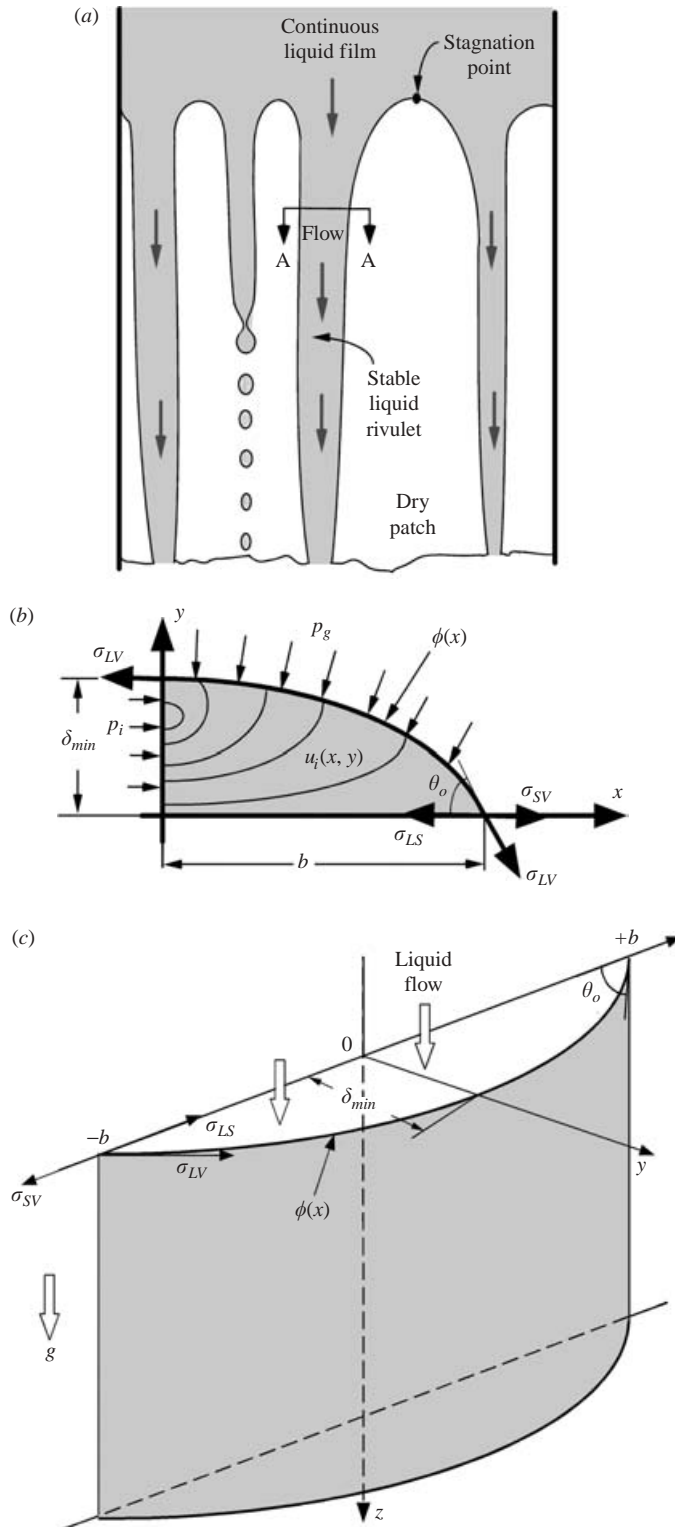


FIGURE 1. Stable rivulets forming following the breakup of a liquid film. (a) Following the breakup of a liquid film: (b) Forces acting on a liquid rivulet (A-A). (c) A stable rivulet flowing down on a vertical surface.

of symmetry has been shown to equal the liquid film thickness at breakup (El-Genk & Saber 2001, 2002). The breakup of a flowing thin liquid film typically occurs when the liquid flow rate decreases below that required to maintain a continuous film on the underlying surface. The liquid flow rate and the film thickness at breakup are known as the minimum wetting rate (MWR) and the minimum liquid film thickness (MLFT), respectively.

Reported analytical approaches for predicting MWR and MLFT for a non-evaporating liquid film, flowing down a vertical surface, are based on either the force balance (FB) at a stagnation point (Hartely & Murgatroyd 1964) on the triple liquid–gas–solid interface or on the minimization of the total energy (MTE) of a stable liquid rivulet, formed following the film breakup (Hobler 1964; Bankoff 1971; Mikielwicz & Moszynski 1976; Doniec 1991). Most reported work to date has been limited to the breakup of a non-evaporating liquid film, flowing down on a vertical surface, with no interfacial shear at the free surface. Table 1 gives the reported analytical expressions for the dimensionless MLFT ($\Delta_{min,o}$) and MWR ($\Gamma_{min,o}$) for such a liquid film. The predictions of the MWR and MLFT using different analytical approaches based on FB and MTE have shown mixed results when compared with experimental data (table 1). These predictions were within -35% to $+42\%$ and within -70% to $+230\%$, respectively, of the reported experimental data for $\Delta_{min,o}$ and $\Gamma_{min,o}$ (Hartely & Murgatroyd 1964; Hobler 1964; Bankoff 1971; Mikielwicz & Moszynski 1976; Doniec 1991) (table 1). However, incorporating a two-dimensional liquid flow velocity and an accurate profile of the stable liquid rivulet in the total energy of the rivulet have been shown to improve the predictions of $\Delta_{min,o}$ and $\Gamma_{min,o}$ markedly to within $\pm 10 - 15\%$ and $\pm 20\%$, respectively, of the reported experimental data for various liquids (El-Genk & Saber 2001).

This paper extends the methodology of El-Genk & Saber (2001) based on the MTE to investigate the breakup of a non-evaporating thin liquid film flowing down or climbing on a vertical or inclined surface and subject to cocurrent or countercurrent interfacial shear (or gas flow). For these conditions, no experimental data have been reported, except for a climbing water film on the inner surface of a vertical acrylic resin tube, driven by an upward air flow (Hewitt & Lacey 1965). These investigators have measured Γ_{min} at breakup and the formation and rewetting of a stable dry patch at different liquid and air flow rates. Analytical expressions for Γ_{min} and the corresponding MLFT, Δ_{min} for a downflowing liquid film subject to either cocurrent or countercurrent gas flow and for a climbing liquid film are developed. These expressions are given in terms of the equilibrium contact angle of the liquid, θ_o , the interfacial shear, τ_i , (or gas velocity, u_g), the inclination angle of the surface from vertical, α_o , and the liquid physical properties. The obtained expressions of Δ_{min} and Γ_{min} for a climbing liquid film are compared with the experimental data of Hewitt & Lacey (1965).

2. Problem statement

The problem investigated in this paper is that of the breakup of a non-evaporating thin liquid film, flowing down or climbing on a vertical or inclined surface and subject to either cocurrent or countercurrent gas flow in a gravitational field (figures 1 and 2). The three cases investigated are: (i) downflowing liquid film subject to a cocurrent gas flow (figure 2a), (ii) downflowing liquid film subject to a countercurrent gas flow (figure 2b), and (iii) climbing liquid film, driven by a upward gas flow (figure 2c). In the first two cases, the gravity force drives the net liquid flow downward, assisted by

| Reference | Expressions | Highlights and assumptions |
|--|---|---|
| Hartely & Murgatroyd (1964) | $\Delta_{min,o} = (1 - \cos \theta_o)^{1/5}$ $\Gamma_{min,o} = 1.693 \Delta_{min,o}^3$ | <p>Based on FB at stagnation point (figure 1). Zero-order velocity approximation. $\Gamma_{min,o}$ based on Nusselt theory approx. far upstream of stagnation point. Overestimate reported data of $\Delta_{min,o}$ and $\Gamma_{min,o}$ by 30% and 70%, respectively.</p> |
| Hobler (1964) | $\Delta_{min,o} = (3/2)^{1/5} (1 - \cos \theta_o)^{1/5}$ | <p>Based on minimization of total energy of a stable liquid rivulet (figure 1). No information on rivulet profile. Zero-order velocity approximation. $\Gamma_{min,o}$ based on Nusselt theory approx. Overestimate reported data of $\Delta_{min,o}$ by 42%.</p> |
| Bankoff (1971); Mikielewicz & Moszynski (1976) | $\Delta_{min,o}^5 + (1 - \cos \theta_o) - G^*(\theta_o) \Delta_{min,o}^3 = 0$ $\Gamma_{min,o} \text{ (derived)} = 1.693 \Delta_{min,o}^3$ | <p>Based on minimization of total energy of a stable liquid rivulet (figure 1). Zero-order liquid velocity approximation. Rivulet profile assumed part of a circle. $\Gamma_{min,o}$ based on Nusselt theory approx. Underestimate reported date of $\Delta_{min,o}$ and $\Gamma_{min,o}$ by 35% and 230%, respectively.</p> |
| Doniec (1991) | $\Delta_{min,o} = (3/7)^{1/5} (1 - \cos \theta_o)^{1/5}$ $\Gamma_{min,o} = 1.693 \Delta_{min,o}^3$ | <p>Based on minimization of total energy of a stable liquid rivulet (figure 1). Zero-order velocity approximation. Rivulet profile determined based on zero-order liquid velocity approximation. $\Gamma_{min,o}$ based on Nusselt theory approx. Overestimate reported date of $\Delta_{min,o}$ and $\Gamma_{min,o}$ by 30% and 50%, respectively.</p> |
| El-Genk & Saber (2001) | $\Delta_{min,o} = (1 - \cos \theta_o)^{0.22}$ $\Gamma_{min,o} = 0.67 \Delta_{min,o}^{2.83} + 0.26 \Delta_{min,o}^{9.51}$ | <p>Based on minimization of total energy of a stable liquid rivulet (figure 1). Two-dimensional velocity distribution $u_l(x, y)$ within stable rivulet (figure 1). Rivulet profile based on $u_l(x, y)$. $\Gamma_{min,o}$ based on the derived two-dimensional velocity distribution in rivulet. Agree with reported data of $\Delta_{min,o}$ and $\Gamma_{min,o}$ to within ± 10–15% and $\pm 20\%$, respectively.</p> |

$$G^*(\theta_o) = \left(\frac{5}{2}\right) \frac{\sin \theta_o}{f(\theta_o)} \left(\frac{2\psi(\theta_o)}{3 \sin \theta_o}\right)^{3/5} \left(\frac{\theta_o}{\sin \theta_o} - \cos \theta_o\right)^{2/5},$$

$$\text{where } f(\theta_o) = -\frac{1}{4} \cos^3 \theta_o \sin \theta_o - \frac{13}{8} \cos \theta_o \sin \theta_o - \frac{3}{2} \theta_o \sin^2 \theta_o + \frac{15}{8} \theta_o,$$

$$\text{and } \psi(\theta_o) = \theta_o \left(\frac{5}{16} + \frac{15}{4} \cos^2 \theta_o + \frac{5}{2} \cos^4 \theta_o\right) - \sin \theta_o \left(\frac{113}{48} \cos \theta_o + \frac{97}{24} \cos^3 \theta_o + \frac{1}{6} \cos^5 \theta_o\right).$$

TABLE 1. Expressions of $\Delta_{min,o}$ and $\Gamma_{min,o}$ for a non-evaporating liquid film flowing down a vertical surface with no interfacial shear.

the cocurrent or opposed by the countercurrent gas flow. In figure 2(c), the countercurrent gas velocity is high enough to derive a climbing liquid film against the gravitational force. Figure 1 shows the static contact angle, θ_o , at the leading edge of a stable liquid rivulet, formed followed the film breakup. This angle is that of the tangent to

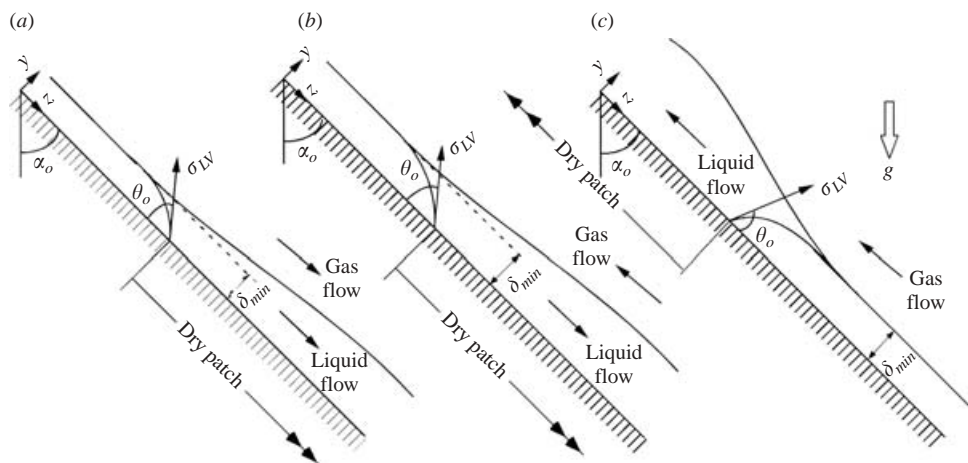


FIGURE 2. Downflowing film subject to (a) cocurrent and (b) countercurrent gas flow. (c) Climbing film subject to cocurrent gas flow.

the liquid–gas interface (figure 1b), or of the surface tension, σ_{LV} , at the liquid–gas interface lines of the rivulet.

Approximate two-dimensional liquid flow velocity distribution in the rivulet, developed based on the Ritz method (Reddy 1984), and a profile of the rivulet are incorporated in the steady-state total energy equation of the rivulet. The minimized total energy and the steady-state momentum balance equations of the liquid rivulet are solved for δ_{min} and γ_{min} . The steady-state total energy equation of the rivulet is presented and discussed next.

3. Energy equation of a stable rivulet

The steady-state total energy, e_{tot} , of a stable liquid rivulet, formed following the breakup of a non-evaporating liquid film, is the sum of the liquid kinetic energy and the interfacial energies at the liquid–vapour (LV) and the liquid–surface (LS) interfaces (figure 1) as (El-Genk & Saber 2001):

$$e_{tot} = 2 \int_0^b \left[\left(\int_0^\phi \frac{1}{2} \rho_l u_l^2(x, y) dy \right) + (\sigma_{LV} \sqrt{1 + (d\phi/dx)^2} - \sigma_{LV} \cos \theta_0 + \sigma_{SV}) \right] dx. \quad (3.1)$$

The first term on the right-hand side is the kinetic energy of the liquid flow in the rivulet and the second term is the sum of the surface energies at LV and LS interfaces. In (3.1), ρ_l , u_l , b and ϕ , are the liquid density, liquid velocity, the liquid rivulet half-width, and the rivulet profile (figures 1b and 1c), respectively, σ_{LV} and σ_{SV} are the surface tension at the LV and surface–vapour (SV) interfaces, respectively, x is the distance, measured from the rivulet’s plane of symmetry, along the surface (figure 1b), and y is the distance normal to the surface. The liquid volumetric flow rate in the rivulet, q , can be expressed as:

$$q = \int_0^b q' dx, \quad (3.2a)$$

where

$$q' = 2 \int_0^\phi u_1(x, y) dy. \quad (3.2b)$$

The steady-state two-dimensional liquid flow velocity in the rivulet, $u_l(x, y)$, is obtained in the next section based on the Ritz method (Reddy 1984) and incorporated into (3.1) and (3.2).

4. Two-dimensional velocity field in a liquid rivulet

For a steady-state incompressible and Newtonian liquid rivulet flow (figures 1a and 1b) on an inclined surface with an angle α_o from vertical (figure 2), the momentum balance equations in the x -, y - and z -directions are given, respectively, as:

$$\frac{\partial p_l}{\partial x} = 0, \quad (4.1a)$$

$$\frac{\partial p_l}{\partial y} = -\rho_l g \sin \alpha_o, \quad (4.1b)$$

$$\frac{\partial^2 u_l(x, y)}{\partial x^2} + \frac{\partial^2 u_l(x, y)}{\partial y^2} = -\frac{g\rho_l}{\mu_l} \cos \alpha_o. \quad (4.1c)$$

In these equations, p_l and μ_l are the liquid pressure and viscosity, respectively, and g is the acceleration due to gravity. Since there is no evaporation from the free surface of the rivulet, the liquid flow in the x - or y -direction is zero, but non-zero in the z -direction (figures 1 and 2). Equation (4.1c) is solved for $u_l(x, y)$, subject to the boundary conditions:

$$u_l(x, 0) = 0, \quad (4.2a)$$

$$\frac{\partial u_l(0, y)}{\partial x} = 0. \quad (4.2b)$$

Equation (4.2a) is for a non-slip condition at the LS interface and (4.2b) indicates a liquid velocity that is maximum at the rivulet's plane of symmetry ($x=0$). An additional boundary condition is required, which is the interfacial shear stress, τ_i , at the LV interface ($y=\phi(x)$) (figure 1b). This boundary condition is expressed as:

$$-\phi'(x) \frac{\partial u_l(x, \phi)}{\partial x} + \frac{\partial u_l(x, \phi)}{\partial y} = -\frac{\tau_i(x)}{\mu_l}. \quad (4.2c)$$

Equations (4.1a–4.1c) are expressed in the following dimensionless form:

$$\frac{\partial P_l}{\partial X} = 0, \quad (4.3a)$$

$$\frac{\partial P_l}{\partial Y} = -\frac{g\delta_{min}^3}{v_l^2} \sin \alpha_o, \quad (4.3b)$$

$$\varepsilon^2 \frac{\partial^2 U_l(x, y)}{\partial X^2} + \frac{\partial^2 U_l(x, y)}{\partial Y^2} = -\cos \alpha_o, \quad (4.3c)$$

and the boundary conditions in (4.2a)–(4.2c) are written in the following dimensionless form:

$$U_l(X, 0) = 0, \quad (4.4a)$$

$$\frac{\partial U_l(0, Y)}{\partial X} = 0, \quad (4.4b)$$

$$-\varepsilon^2 \Phi'(X) \frac{\partial U_l(X, \Phi)}{\partial X} + \frac{\partial U_l(X, \Phi)}{\partial Y} = -\hat{\tau}_i(X)/\Delta_{min}. \quad (4.4c)$$

In these equations, $U_l = (u_l \mu_l / (g \rho_l \delta_{min}^2))$, ε is the aspect ratio of the rivulet (δ_{min}/b), Φ is the dimensionless rivulet profile (ϕ/δ_{min}), X is the dimensionless distance along the solid surface (x/b), and Y is the dimensionless distance in the rivulet normal to the underlying surface (y/δ_{min}), Δ_{min} is the dimensionless minimum liquid film thickness at breakup (δ_{min}/δ^*), δ^* is a characteristic film thickness $= ((15\mu_l^2 \sigma_{LV} / (\rho_l^3 g^2))^{0.2})$, P_l is the dimensionless liquid pressure in the rivulet ($p_l / (\mu_l^2 / (\rho_l \delta_{min}^2))$), and $\hat{\tau}_i$ is the dimensionless interfacial shear stress ($\tau_i / (\rho_l g \delta^*)$) at the free surface of the liquid film. Equation (4.3c), subject to the boundary conditions given by (4.4a)–(4.4c), represents a nonlinear problem for which an analytical solution for $U_l(X, \Phi)$ is not readily available. An approximate analytical solution is obtained using the Ritz method (Reddy 1984; El-Genk & Saber 2001).

When (4.3c) is multiplied by a test function Ω and integrated over the rivulet domain it yields:

$$\int_0^1 \int_0^\Phi \Omega \left(\varepsilon^2 \frac{\partial^2 U_l(X, Y)}{\partial X^2} + \frac{\partial^2 U_l(X, Y)}{\partial Y^2} + \cos \alpha_o \right) dY dX = 0. \quad (4.5)$$

The integration of (4.5) and the application of the boundary conditions ((4.4a)–(4.4c)) give:

$$\int_0^1 \int_0^\Phi \left(\varepsilon^2 \frac{\partial \Omega}{\partial X} \frac{\partial U_l}{\partial X} + \frac{\partial \Omega}{\partial Y} \frac{\partial U_l}{\partial Y} \right) dY dX = \int_0^1 \int_0^\Phi \Omega \cos \alpha_o dY dX - \int_0^1 \Omega \frac{\hat{\tau}_i(X)}{\Delta_{min}} \sqrt{1 + \varepsilon^2 \Phi'^2(X)} dX. \quad (4.6)$$

According to the Ritz method (Reddy 1984), the two-dimensional liquid velocity in the rivulet, U_l , may be expressed in the form of a finite series as:

$$U_l(X, Y) = \eta_o + \sum_{i=1}^m c_i \eta_i(X, Y). \quad (4.7)$$

The application of the boundary condition (4.4a) shows that the selected function, η_o , is zero, and the liquid velocity can be expressed as:

$$U_l(X, Y) = \sum_{i=1}^m c_i \eta_i(X, Y). \quad (4.8)$$

The assumed functions η_i ($i = 1, 2, \dots, m$) are expressed (El-Genk & Saber 2001) as:

$$\eta_i(X, Y) = \cos \frac{(2i-1)\alpha}{2} X \sin i\alpha Y. \quad (4.9)$$

In (4.9), α is an arbitrary coefficient that affects the conversion of the solution for the liquid velocity in the rivulet. It has been found that, with $\alpha = 0.05$ only three terms in (4.8), or $m = 3$ (El-Genk & Saber 2001), are adequate to obtain an accurate velocity distribution. The obtained velocity distribution using (4.8) and (4.9) in a liquid rivulet flowing down a vertical surface, $\alpha_o = 0^\circ$, with no interfacial shear (El-Genk & Saber 2001) has been shown to be in excellent agreement with the numerical solution of Allen & Biggin (1974). This agreement confirmed the suitability of (4.9) for calculating liquid flow in the rivulet.

The Ritz coefficients, c_i ($i = 1, 2, \dots, m$) in (4.8), obtained from substituting (4.8) and (4.9) into (4.6), are expressed in a matrix form as:

$$\begin{bmatrix} b_{11} & b_{12} & \dots & \dots & b_{1n} \\ b_{21} & b_{22} & \dots & \dots & b_{2n} \\ \dots & \dots & \dots & \dots & \dots \\ \dots & \dots & \dots & \dots & \dots \\ b_{n1} & b_{n2} & \dots & \dots & b_{nn} \end{bmatrix} \begin{Bmatrix} c_1 \\ c_2 \\ \dots \\ \dots \\ c_n \end{Bmatrix} = \begin{Bmatrix} l_1 \\ l_2 \\ \dots \\ \dots \\ l_n \end{Bmatrix}. \quad (4.10)$$

The terms b_{ij} and l_i in (4.10) are given as:

$$b_{ij} = \int_0^1 \int_0^\Phi \left(\varepsilon \frac{\partial \eta_i(X, Y)}{\partial X} \frac{\partial \eta_j(X, Y)}{\partial X} + \frac{\partial \eta_i(X, Y)}{\partial Y} \frac{\partial \eta_j(X, Y)}{\partial Y} \right) dY dX, \quad (4.11)$$

$$l_i = \int_0^1 \int_0^\Phi \eta_i(X, Y) \cos \alpha_o dY dX - \int_0^1 \eta_i(X, \Phi) \frac{\hat{\tau}_i(X)}{\Delta_{min}} \sqrt{1 + \varepsilon \Phi'^2(X)} dX. \quad (4.12)$$

The second term on the right-hand side of (4.12) is the contribution of the interfacial shear at the free surface of the liquid rivulet. For a downflowing liquid rivulet on a vertical surface ($\alpha_o = 0$), with no interfacial shear, this term drops out (El-Genk & Saber 2001). The integrals in (4.11) and (4.12) are evaluated numerically, after substituting expressions for the rivulet profile, $\Phi(X)$ and the interfacial shear stress, $\hat{\tau}_i(X)$, which are presented and discussed in the next two sections.

5. Rivulet profile

The liquid pressure along the LV interface of the rivulet, $p_l(y = \phi)$, is obtained from integrating (4.1b) with respect to y , as:

$$p_l(y = \phi) = p_{LS} - \rho_l g \phi \sin \alpha. \quad (5.1)$$

The liquid pressure at the LS interface, p_{LS} , is independent of x . Another expression for $p_l(y = \phi)$ is obtained in terms of the pressure of the gas surrounding the rivulet, p_v , using the well-known Laplace relation as:

$$p_l(y = \phi) - p_v = \frac{\sigma_{LV}}{r} \quad \text{where} \quad \frac{1}{r} = k = -\frac{\phi''(x)}{(1 + \phi'^2(x))^{3/2}}. \quad (5.2)$$

The force balances in the x - and y -directions (figure 1b) give the following expressions for the gas pressure and the liquid pressure in the rivulet at the LS interface (Allen & Biggin 1974) as:

$$\left. \begin{aligned} p_v &= p_l(y = \delta_{min}) + \frac{1}{2} \rho_l g \delta_{min} \sin \alpha_o - \frac{\sigma_{LV}(1 - \cos \theta_o)}{\delta_{min}}, \\ p_{LS} &= p_v + \frac{1}{2} \frac{\rho_l g A \sin \alpha_o}{b} + \frac{\sigma_{LV} \sin \theta_o}{b}. \end{aligned} \right\} \quad (5.3)$$

Eliminating $p_l(y = \phi)$ from (5.1) and (5.2) and substituting for p_v and p_{LS} from (5.3) gives the following nonlinear second-order ordinary differential equation:

$$\frac{\phi''(x)}{(1 + \phi'^2(x))^{3/2}} = \frac{\rho_l g \sin \alpha_o}{\sigma_{LV}} \phi(x) - \left(\frac{\rho_l g \delta_{min} \sin \alpha_o}{2\sigma_{LV}} + \frac{(1 - \cos \theta_o)}{\delta_{min}} \right). \quad (5.4)$$

This equation is solved analytically for the rivulet profile, $\phi(x)$, subject to the following boundary conditions:

$$\phi(x = 0) = \delta_{min}, \quad \phi'(x = 0) = 0, \quad (5.5a)$$

$$\phi(x = b) = 0, \quad \phi'(x = b) = -\tan \theta_o. \quad (5.5b)$$

Equations (5.4) and (5.5) are rewritten in a dimensionless form as:

$$\frac{\Phi''(X)}{(1 + \varepsilon^2 \Phi'^2(X))^{3/2}} = \frac{\rho_l g b^2 \sin \alpha_o}{\sigma_{LV}} \Phi(X) - \left(\frac{\rho_l g b^2 \sin \alpha_o}{2\sigma_{LV}} + \frac{(1 - \cos \theta_o)}{\varepsilon^2} \right), \quad (5.6)$$

and

$$\Phi(X = 0) = 1, \quad \Phi'(X = 0) = 0, \quad (5.7a)$$

$$\Phi(X = 1) = 0, \quad \Phi'(X = 1) = -\frac{1}{\varepsilon} \tan \theta_o. \quad (5.7b)$$

Substituting $\Phi'' = \Phi' d\Phi'/d\Phi$ into (5.6), the resulting equation is expressed in an integral form as:

$$\int_0^{\Phi'} \frac{\Phi' d\Phi'}{(1 + \varepsilon^2 \Phi'^2)^{3/2}} = \int_1^{\Phi} \left(\frac{\rho_l g b^2 \sin \alpha_o}{\sigma_{LV}} \Phi - \left(\frac{\rho_l g b^2 \sin \alpha_o}{2\sigma_{LV}} + \frac{(1 - \cos \theta_o)}{\varepsilon^2} \right) \right) d\Phi. \quad (5.8)$$

This equation gives:

$$\frac{1}{(1 + \varepsilon^2 \Phi'^2)^{1/2}} = 1 + \frac{1}{2} \alpha_1 (1 - \Phi^2) - \alpha_2 (1 - \Phi), \quad (5.9)$$

where

$$\alpha_1 = \frac{\rho_l g \delta_{min}^2 \sin \alpha_o}{\sigma_{LV}}, \quad \alpha_2 = \frac{\rho_l g \delta_{min}^2 \sin \alpha_o}{2\sigma_{LV}} + (1 - \cos \theta_o). \quad (5.10)$$

Substituting:

$$\Phi' = \frac{1}{\varepsilon} \tan 2\xi, \quad (5.11)$$

into (5.9), yields:

$$1 + \frac{1}{2} \alpha_1 (1 - \Phi^2) - \alpha_2 (1 - \Phi) = -\cos 2\xi. \quad (5.12)$$

Differentiating (5.12) with respect to Φ gives:

$$\alpha_2 - \alpha_1 \Phi = 2 \sin 2\xi \frac{d\xi}{dX} / \Phi'. \quad (5.13)$$

The quadratic solution of (5.12) yields:

$$\alpha_2 - \alpha_1 \Phi = \frac{2\sqrt{\alpha_1}}{\sin \beta} \sqrt{1 - \sin^2 \beta \sin^2 \xi}, \quad (5.14)$$

where

$$\kappa^2 = \sin^2 \beta = \frac{4\alpha_1}{(\alpha_2 - \alpha_1)^2 + 4\alpha_1}. \quad (5.15)$$

Substituting Φ' from (5.11) into (5.13), and equating the result with (5.14) gives:

$$\frac{d\xi}{dX} = \frac{\sqrt{\alpha_1}}{\varepsilon \sin \beta} \frac{\sqrt{1 - \sin^2 \beta \sin^2 \xi}}{1 - 2 \sin^2 \xi}. \quad (5.16)$$

According to the boundary conditions (5.7a) and (5.7b), ξ changes from $\pi/2$ to $(\pi - \theta_o)/2$ as X increases from 0 to 1 (figure 1). The integration of (5.16) with respect to ξ , gives:

$$\begin{aligned} \int_0^X dX &= \int_{\pi/2}^{\xi} \frac{\varepsilon \sin \beta}{\sqrt{\alpha_1}} \frac{1 - 2 \sin^2 \xi}{\sqrt{1 - \sin^2 \beta \sin^2 \xi}} d\xi \\ &= \frac{\varepsilon}{\sqrt{\alpha_1}} \left[\frac{2}{\kappa} \int_{\pi/2}^{\xi} \sqrt{1 - \kappa^2 \sin^2 \xi} d\xi - \left(\frac{2 - \kappa^2}{\kappa} \right) \int_{\pi/2}^{\xi} \frac{d\xi}{\sqrt{1 - \kappa^2 \sin^2 \xi}} \right]. \quad (5.17) \end{aligned}$$

This equation can be rewritten as:

$$X = \frac{\varepsilon}{\sqrt{\alpha_1}} \left[\left(\frac{2 - \kappa^2}{\kappa} \right) (F(\kappa, \pi/2) - F(\kappa, \xi)) - \frac{2}{\kappa} (E(\kappa, \pi/2) - E(\kappa, \xi)) \right]. \quad (5.18)$$

In (5.18), the elliptic integrals of the first and second kinds, $F(\kappa, \xi)$ and $E(\kappa, \xi)$, are given, respectively, as:

$$F(\kappa, \xi) = \int_0^\xi \frac{d\xi}{\sqrt{1 - \kappa^2 \sin^2 \xi}}, \quad E(\kappa, \xi) = \int_0^\xi \sqrt{1 - \kappa^2 \sin^2 \xi} d\xi. \quad (5.19)$$

Equation (5.14) is rearranged to give the following dimensionless profile of the rivulet, $\Phi(X)$, in terms of ξ ((5.16)) as:

$$\Phi(X) = \frac{\alpha_2}{\alpha_1} - \frac{2}{\kappa \sqrt{\alpha_1}} \sqrt{1 - \kappa^2 \sin^2 \xi}, \quad (5.20)$$

where the coefficients α_1 and α_2 are given in (5.10). This liquid rivulet profile is identical to that obtained earlier by El-Genk & Saber (2001) for a non-evaporating stable liquid rivulet flowing down on a vertical surface ($\alpha_o = 0$). The expression for interfacial shear stress at the free surface of the rivulet in terms of the cocurrent and countercurrent gas velocity is discussed next.

6. Interfacial shear stress

The interfacial shear stress at the free surface of the liquid rivulet is given in terms of the gas velocity, u_g , and the interfacial liquid velocity, u_i (Lee & Bankoff 1983) as:

$$\tau_i(x) = 0.5 f_{ia}(x) \rho_g (u_g \pm u_i(x))^2. \quad (6.1)$$

In this equation, the negative and positive signs of u_i , indicate cocurrent and countercurrent interfacial shear (or gas flow), respectively, ρ_g is the gas density, and f_{ia} is the adiabatic friction coefficient. Equation (6.1) is rewritten in a dimensionless form as:

$$\begin{aligned} \hat{\tau}_i(X) &= 0.5 f_{ia}(X) \Delta_{min}^4 \frac{\rho_g}{\rho_l} \left(\frac{\delta^{*3} g}{\nu_l^2} \right) (U_g \pm U_i(X))^2 \\ &= 0.5 f_{ia}(X) \frac{\rho_g}{\rho_l} \left(\frac{\delta^{*3} g}{\nu_l^2} \right) (U_g^* \pm U_i^*(X))^2, \end{aligned} \quad (6.2)$$

where, U_i^* is a dimensionless velocity ($u_i \nu_l / (g \delta^{*2})$) and ν_l is the liquid kinematic viscosity. The adiabatic friction coefficient, $f_{ia}(X)$, is evaluated using the following expression proposed by Grolmes Lambert & Fauske (1974) as:

$$f_{ia}(X) = 0.006 + \bar{A} \delta_{min}^2 \Phi^2(X) (\mu_l / \mu_R)^{-0.44}, \quad (6.3)$$

where, $\bar{A} = 2 \times 10^6 \text{ m}^{-2}$, and μ_R is a reference liquid viscosity = 1.0 cP.

7. Minimization of the liquid rivulet total energy

The obtained steady-state two-dimensional liquid velocity in the rivulet, $u_l(x, y)$ (equation (4.8)) and the rivulet profile, $\phi(x)$ (equation (5.20)) are substituted into the total energy equation of the liquid rivulet (equation (3.1)). This total energy is then minimized to obtain an expression for the liquid film thickness at breakup, Δ_{min} .

The detailed methodology for the minimization of the total energy of the rivulet is presented elsewhere (El-Genk & Saber 2001) and will not be repeated here.

The obtained analytical expression for Δ_{min} is as follows:

$$\Delta_{min} = (a_2(1 - \cos \theta_o)/(a_3 a_1 - 7.5\omega a_2))^{1/5}, \quad (7.1)$$

where the coefficients ω and a_{1-3} in (7.1) are given as:

$$\begin{aligned} \omega = \sum_{i=1}^2 c_i^2 \left(\frac{1}{2} - \frac{1}{4i\alpha} \sin 2i\alpha \right) + 2 \frac{c_1 c_2}{\alpha} \left(\frac{1}{2} \sin \alpha - \frac{1}{6} \sin 3\alpha \right) \\ + 2 \frac{c_1 c_3}{\alpha} \left(\frac{1}{4} \sin 2\alpha - \frac{1}{8} \sin 4\alpha \right) + 2 \frac{c_2 c_3}{\alpha} \left(\frac{1}{2} \sin \alpha - \frac{1}{10} \sin 5\alpha \right), \end{aligned} \quad (7.2a)$$

$$\begin{aligned} a_1 = \sum_i^3 c_i^2 \left(2i\alpha \sin 2i\alpha + 2\varepsilon \left(\frac{(2i-1)\alpha}{2} \right)^2 \frac{1 - \cos 2i\alpha}{1 - \cos \theta_o} \right) \\ + 2c_1 c_2 \left((3\alpha \sin 3\alpha - \alpha \sin \alpha) + 10\varepsilon \left(\frac{\alpha}{2} \right)^2 \frac{\cos \alpha - \cos 3\alpha}{1 - \cos \theta_o} \right) \\ + 2c_1 c_3 \left((4\alpha \sin 4\alpha - 2\alpha \sin 2\alpha) + 26\varepsilon \left(\frac{\alpha}{2} \right)^2 \frac{\cos 2\alpha - \cos 4\alpha}{1 - \cos \theta_o} \right) \\ + 2c_2 c_3 \left((5\alpha \sin 5\alpha - \alpha \sin \alpha) + 34\varepsilon \left(\frac{\alpha}{2} \right)^2 \frac{\cos \alpha - \cos 5\alpha}{1 - \cos \theta_o} \right), \end{aligned} \quad (7.2b)$$

$$a_2 = \sum_i^3 c_i \left(i\alpha \cos i\alpha + \varepsilon \left(\frac{(2i-1)\alpha}{2} \right)^2 \frac{\sin i\alpha}{1 - \cos \theta_o} \right), \quad (7.2c)$$

$$a_3 = \sum_{i=1}^3 \frac{c_i}{i\alpha} (1 - \cos i\alpha). \quad (7.2d)$$

The minimum wetting rate, Γ_{min} , is obtained from the integration of (3.2), after substituting the steady-state two-dimensional liquid velocity in the rivulet, $U_l(X, Y)$ from (4.8), and the rivulet profile, $\Phi(X)$ from (5.20). The expression obtained is as follows:

$$\Gamma_{min} = (15)^{3/5} \left(\frac{a_2(1 - \cos \theta_o)}{a_3 a_1 - \frac{15}{2}\omega a_2} \right)^{3/5} \int_0^1 \sum_{i=1}^3 \frac{c_i}{i\alpha} \cos \frac{(2i-1)\alpha}{2} X (1 - \cos i\alpha \Phi) dX. \quad (7.3)$$

Equations (7.1) and (7.3) show that when the equilibrium contact angle $\theta_o > 0^\circ$, there is only one real solution for each of Δ_{min} and Γ_{min} . For a perfectly wetting liquid, ($\theta_o = 0$), both Δ_{min} and Γ_{min} are zero.

8. Results and discussion

Figures 3 and 4 compare the expressions obtained for Δ_{min} and Γ_{min} in (7.1) and (7.3), respectively, with the reported experimental data for a climbing water film (Hewitt & Lacey 1965). In the experiments, air entered through the bottom of a vertical acrylic-resin tube, 31.75 mm in inner diameter, and water entered the tube through a porous section in the wall. The upward air and water film flow rates were independently increased up to 227.3 kg h⁻¹ and 8.2 kg h⁻¹, respectively. For a given air flow rate, the water flow rate was first set well above Γ_{min} , then reduced in successive

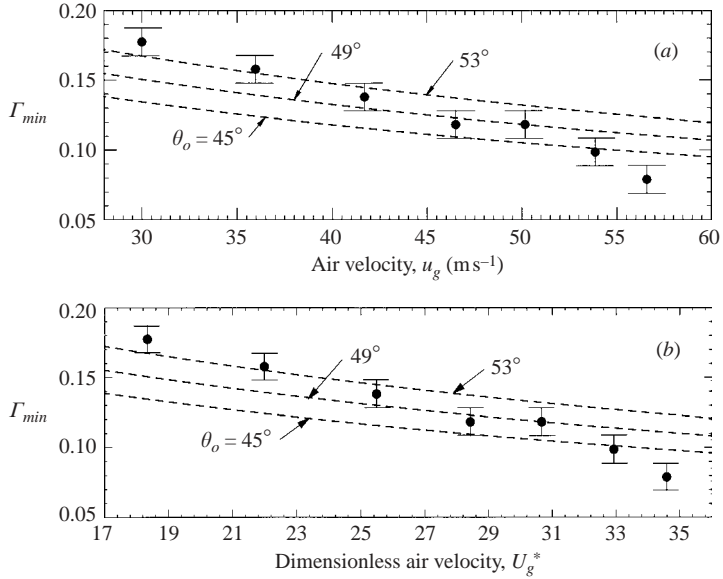


FIGURE 3. Comparison of ---, present predictions of Γ_{min} with ●, experimental data for a climbing water film (Hewitt & Lacey 1965).

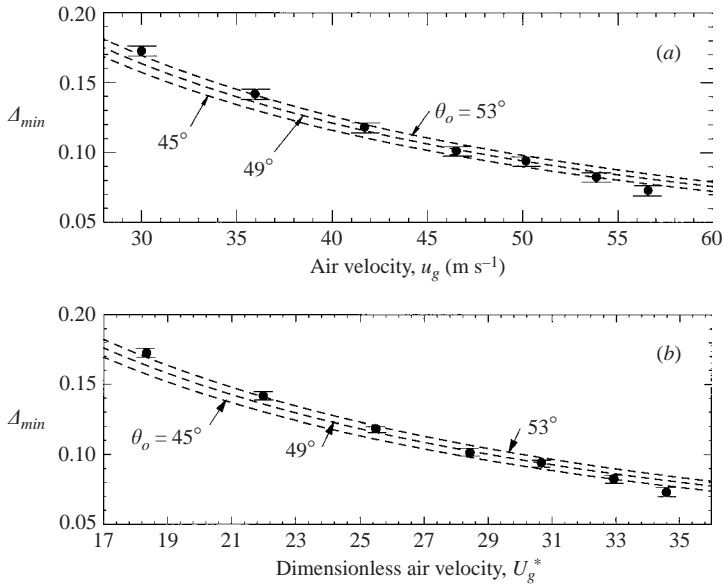


FIGURE 4. Comparison of ---, the predictions of Δ_{min} with ●, the experimental data for a climbing water film (Hewitt & Lacey 1965).

increments of 0.9 kg h^{-1} , until a stable dry patch was formed. The dry patch was produced using an air jet from a capillary tube. If the dry patch was rewetted on the cessation of the air jet, the water flow rate was reduced again and the procedures were repeated until a stable dry patch was formed. The corresponding water flow rate in the climbing film was taken as the minimum wetting rate for the formation of a stable dry patch, which represents a lower value for the liquid film breakup. The measured

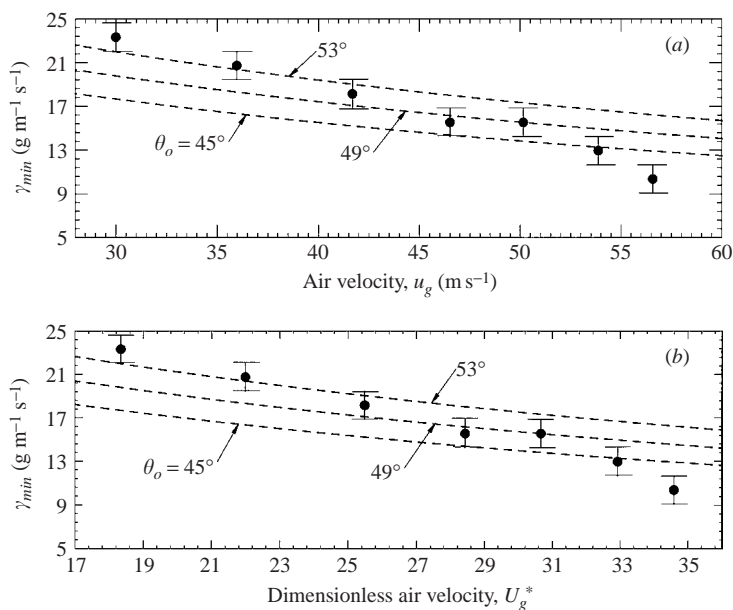


FIGURE 5. Comparison of ---, present predictions of γ_{min} ($\text{g m}^{-1} \text{s}^{-1}$) with ●, experimental data for a climbing water film (Hewitt & Lacey 1965).

water flow rate for rewetting the stable dry patch represents an upper limit for the liquid film breakup. Therefore, the exact value of the minimum wetting rate at the breakup of the climbing water film in the experiments is in between those measured for the formation and the rewetting of a dry patch. The bar-lines in figure 3 connect the measured values of Γ_{min} for the formation and for the rewetting of a stable dry patch (Hewitt & Lacey 1965). The averages of these two values, indicated by the solid circle symbols in figure 3, are taken as Γ_{min} for the breakup of the climbing water film in the experiments.

The predictions in figures 3–6 used the measured equilibrium contact angle, θ_o , by Hewitt & Lacey (1965) for the water/acrylic-resin-tube/air system using the sessile drop method, which averaged $49^\circ \pm 4^\circ$. The data in figures 3(a) and 3(b) are for upward airflow rates $> 91 \text{ kg h}^{-1}$ ($u_g > 28 \text{ m s}^{-1}$ or $U_g^* > 17$) and water flow rates $< 8 \text{ kg h}^{-1}$ (or $\gamma_{min} < 25 \text{ g m}^{-1} \text{s}^{-1}$) (Hewitt & Lacey 1965). At these flow rates, the water entrainment in the airflow was minimal.

Figure 3 compares the values of Γ_{min} for the breakup of the climbing water film in Hewitt & Lacey (1965) experiments (solid circle symbols) with those calculated using (7.3), while figure 4 compares the corresponding values of Δ_{min} , with those calculated using (7.1). The calculated values of Γ_{min} and Δ_{min} in figures 3 and 4, respectively, for three equilibrium contact angles, $\theta_o = 45^\circ$ ($49 - 4^\circ$), 49° , and 53° ($49 + 4^\circ$), indicate excellent agreement with the experimental data of Hewitt & Lacey (1965). When $u_g > 55 \text{ m s}^{-1}$ (or $U_g^* > 33.6$), the experimental values of Γ_{min} and Δ_{min} are lower than the present predictions, which may be attributed to a liquid evaporation in the experiments. The results show that both Γ_{min} and Δ_{min} decrease as the upward air velocity increases. However, the relative decrease in Δ_{min} with increasing airflow velocity is much larger than in the Γ_{min} (figures 3 and 4).

Figures 5 and 6 also compare the present predictions for γ_{min} and δ_{min} with the reported measurements by Hewitt & Lacey (1965). When $\theta_o = 49^\circ$, the thickness of

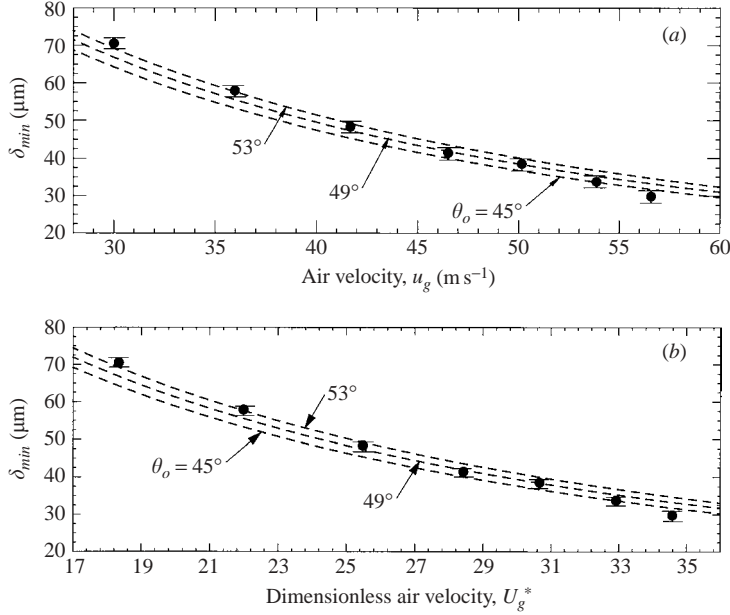


FIGURE 6. Comparison of ---, present predictions of δ_{min} (μm) with \bullet , experimental data for a climbing water film (Hewitt & Lacey 1965).

the climbing water film at the breakup and the formation of a stable dry patch in the experiments, decreased from $\sim 67 \mu\text{m}$ to $31 \mu\text{m}$, as the upward airflow velocity was increased from 30 to 60 m s^{-1} (or U_g^* from 18.3 to 36.7). Also, the value of γ_{min} decreased from $20 \text{ g m}^{-1} \text{ s}^{-1}$ at an air velocity of 30 m s^{-1} to $13.6 \text{ g m}^{-1} \text{ s}^{-1}$ at a higher air velocity of 60 m s^{-1} (figure 5).

8.1. Effect of inclination angle for zero interfacial shear

For a zero gas velocity, $U_g^* = 0$, the rivulet profile is obtained using (5.18) and (5.20) in conjunction with (7.1). The calculated profiles for an equilibrium contact angle, $\theta_o = 45^\circ$, and different inclination angles ($\alpha_o = 0^\circ, 30^\circ, 60^\circ, 70^\circ$ and 80°) are delineated in figure 7. The solid circle symbols indicate the profile of a stable rivulet flowing down on a vertical surface ($\alpha_o = 0$) with no interfacial shear (El-Genk & Saber 2001). Figure 7 shows that the thickness of the liquid rivulet at the plane of symmetry ($X = 0$), which is equal to the liquid film thickness at breakup, increases as α_o increases. For example, increasing α_o from 0° to 60° increase the dimensionless liquid film thickness at breakup, $\Delta_{min,\alpha}$ (or $\phi(x)/\delta^*$), without interfacial shear from 0.76 to 1.01 , respectively. The higher value of $\Delta_{min,\alpha}$ at $\alpha_o = 60^\circ$ is caused by the decrease in the gravity tangential component affecting the liquid film flow.

Figures 8(a) and 8(b) show the effects of both the equilibrium contact angle, θ_o , and the inclination angle, α_o , on the liquid-film thickness and the corresponding wetting rate at breakup, $\Delta_{min,\alpha}$ and $\Gamma_{min,\alpha}$, respectively, for zero interfacial shear. For a vertical surface ($\alpha_o = 0$), the calculated values of $\Delta_{min,o}$ and $\Gamma_{min,o}$ have been empirically correlated solely in terms of θ_o as (El-Genk & Saber 2001):

$$\Delta_{min,o} = (1 - \cos \theta_o)^{0.22}, \quad (8.1a)$$

$$\Gamma_{min,o} = 0.67 \Delta_{min,o}^{2.83} + 0.26 \Delta_{min,o}^{9.51}. \quad (8.1b)$$

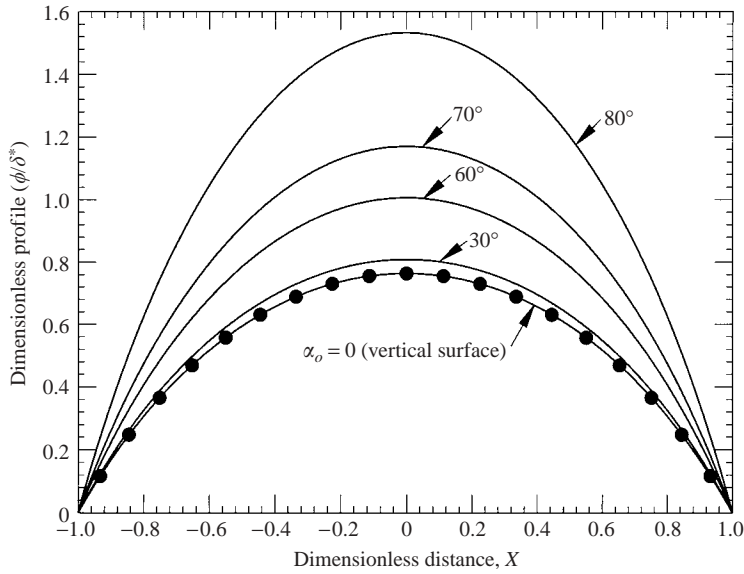


FIGURE 7. Calculated rivulet profiles for different inclination angles, $\theta_o = 45^\circ$, and zero interfacial shear. —, present predictions, (5.18) and (5.20); ●, El-Genk & Saber (2001) ($\alpha_o = 0$).

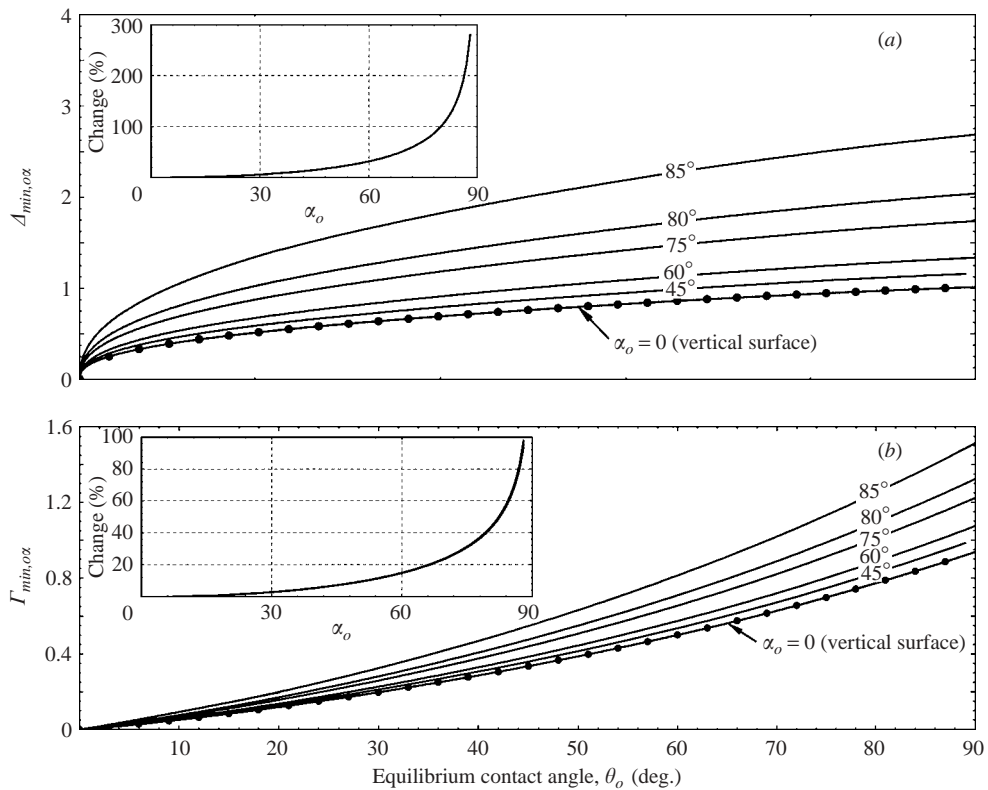


FIGURE 8. Effect of inclination and equilibrium contact angles on (a) $\Delta_{min,ox}$ and (b) $\Gamma_{min,ox}$ in the absence of interfacial shear. ●, El-Genk & Saber (2001), $\alpha_o = 0$. (a) —, present (7.1); (b) —, present (7.3).

Equations (8.1a) and (8.1b) are similar to those reported by earlier investigators and given in table 1, except that the values of the exponents and the coefficients are different. Equations (8.1a) and (8.1b) have been shown to agree to within $\pm 10\text{--}15\%$ and $\pm 20\%$ with the reported measurements for the breakup of downflowing films of water and water–glycerol mixtures on vertical glass, copper, Perspex and stainless steel surfaces (El-Genk & Saber 2001).

The calculated values of $\Delta_{min,\alpha}$ and $\Gamma_{min,\alpha}$, for a liquid film flowing down an inclined surface with no interfacial shear, increase as either the equilibrium contact angle, θ_o , or the inclination angle of the underlying surface, α_o , increases (figures 8a and 8b). For example, when $\theta_o = 45^\circ$, increasing α_o from 0° (vertical surface) to 85° , increases $\Delta_{min,\alpha}$ and $\Gamma_{min,\alpha}$ by $\sim 166\%$ and 64% , respectively. The two inserts in figures 8(a) and 8(b) show the estimated percentage increases in $\Delta_{min,\alpha}$ and $\Gamma_{min,\alpha}$, respectively, as the inclination angle, α_o , increases from 0° to 85° . The obtained values of $\Delta_{min,\alpha}$ and $\Gamma_{min,\alpha}$ are empirically correlated in terms of those for a vertical surface and with no interfacial shear, $\Delta_{min,o}$ and $\Gamma_{min,o}$ respectively, and α_o , as:

$$\Delta_{min,\alpha} = \Delta_{min,o}(\cos \alpha_o)^{-0.4}, \quad (8.2a)$$

$$\Gamma_{min,\alpha} = \Gamma_{min,o}(\cos \alpha_o)^{-0.2}. \quad (8.2b)$$

These expressions are much simpler and within $\pm 1\%$ of the values calculated using (7.1) and (7.3). In (8.2a) and (8.2b), $\Delta_{min,o}$ and $\Gamma_{min,o}$ represent the contributions of the equilibrium contact angle, θ_o , while $(\cos \alpha_o)^{-0.4}$ and $(\cos \alpha_o)^{-0.2}$ represent the contributions of the inclination angle on $\Delta_{min,\alpha}$ and $\Gamma_{min,\alpha}$, respectively. The results on the effect of applying a cocurrent interfacial shear (or gas flow) on both Δ_{min} and Γ_{min} for a liquid film flowing down an inclined surface are presented and discussed next.

8.2. Effects of cocurrent interfacial shear (or gas flow)

The results of the breakup of a thin non-evaporating liquid film, flowing down an inclined surface and subject to a cocurrent gas flow (figure 2a) are presented in figures 9(a) and 9(b). The ratios of the liquid film thickness at breakup, Δ_{min} , and of the corresponding wetting rate, Γ_{min} , to those given by (8.2a) and (8.2b), respectively, are plotted versus $[U_g^{*0.94}(1 - \cos \theta_o)^{0.16}]$. The calculated values of $[\Delta_{min}/\Delta_{min,\alpha}]$ and $[\Gamma_{min}/\Gamma_{min,\alpha}]$ for all inclination and equilibrium contact angles collapse nicely. The inserts in figures 9(a) and 9(b) show that both $[\Delta_{min}/\Delta_{min,\alpha}]$ and $[\Gamma_{min}/\Gamma_{min,\alpha}]$ drop below unity (corresponding to a zero interfacial shear) as the dimensionless gas velocity, U_g^* , increases. For example, when $\theta_o = 45^\circ$, increasing U_g^* from zero (no interfacial shear stress) to 3 decreases $[\Delta_{min}/\Delta_{min,\alpha}]$ and $[\Gamma_{min}/\Gamma_{min,\alpha}]$ to 0.68 and 0.72, respectively. For a given gas velocity, increasing θ_o decreases both $[\Delta_{min}/\Delta_{min,\alpha}]$ and $[\Gamma_{min}/\Gamma_{min,\alpha}]$, but $\Delta_{min,\alpha}$ and $\Gamma_{min,\alpha}$ increase as θ_o increases (figures 8a and 8b). The calculated values of $[\Delta_{min}/\Delta_{min,\alpha}]$ and $[\Gamma_{min}/\Gamma_{min,\alpha}]$ are empirically correlated as:

$$\Delta_{min}/\Delta_{min,\alpha} = 1 - 0.794(U_g^{*1.462}(1 - \cos \theta_o)^{0.249}) + 0.661(U_g^{*1.538}(1 - \cos \theta_o)^{0.262}), \quad (8.3a)$$

$$\Gamma_{min}/\Gamma_{min,\alpha} = 1 + 0.897(U_g^{*1.445}(1 - \cos \theta_o)^{0.246}) - 1.025(U_g^{*1.388}(1 - \cos \theta_o)^{0.236}). \quad (8.3b)$$

These empirical expressions, indicated in figures 9(a) and 9(b) by the solid lines, are within $\pm 2\%$ of the calculated values using (7.1) and (7.3), respectively.

8.3. Effects of countercurrent shear stress (or gas flow)

Figures 10(a) and 10(b) present the results of the breakup of a liquid film flowing down an inclined surface and subject to a countercurrent interfacial shear or gas flow

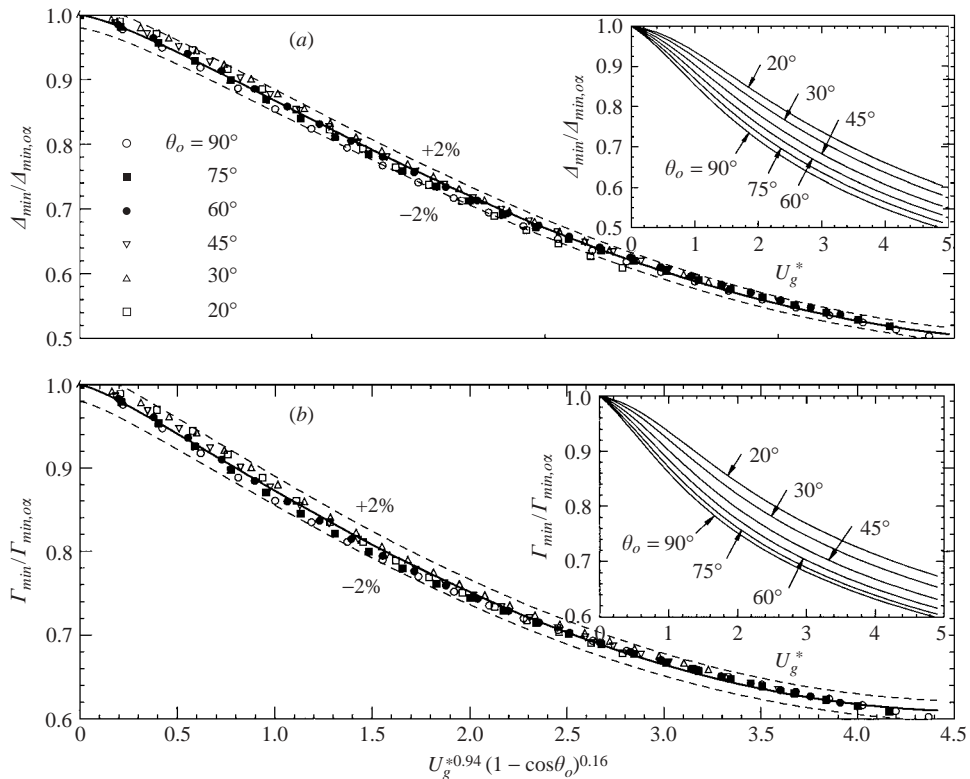


FIGURE 9. Effects of gas velocity and equilibrium contact angle on (a) Δ_{min} and (b) Γ_{min} for a downflowing liquid film, subject to cocurrent interfacial shear.

(figure 2b). These figures show that the ratios $[\Delta_{min}/\Delta_{min,\alpha}]$ and $[\Gamma_{min}/\Gamma_{min,\alpha}]$ are not only greater than unity, but also increase as either U_g^* or θ_o increases (see the inserts in figures 10a and 10b); ratios of unity correspond to a zero interfacial shear (or gas velocity). When $\theta_o = 45^\circ$, the same as that measured by Hewitt & Lacy (1956), increasing U_g^* from zero (no interfacial shear) to unity increases $[\Delta_{min}/\Delta_{min,\alpha}]$ and $[\Gamma_{min}/\Gamma_{min,\alpha}]$ by 22% and 27%, respectively (see inserts in figures 10a and 10b). The calculated values of $[\Delta_{min}/\Delta_{min,\alpha}]$ and $[\Gamma_{min}/\Gamma_{min,\alpha}]$ for a liquid film flowing down an inclined surface and subject to a countercurrent interfacial shear (figure 2b) are empirically correlated, respectively, as:

$$\Delta_{min}/\Delta_{min,\alpha} = 1 + 0.515U_g^{*2.27}(1 - \cos\theta_o)^{0.651}, \quad (8.4a)$$

$$\Gamma_{min}/\Gamma_{min,\alpha} = 1 + 0.473(U_g^{*1.938}(1 - \cos\theta_o)^{0.556}) + 1.331(U_g^{*9.172}(1 - \cos\theta_o)^{2.632}). \quad (8.4b)$$

These expressions, indicated in figures 10(a) and 10(b) by solid lines, are within $\pm 2\%$ of the calculated values using (7.1) and (7.3). The following section presents and discusses the obtained velocity fields in stable liquid rivulets for the three cases delineated in figures 2(a)–2(c).

8.4. Liquid velocity field in a stable rivulet

Figures 11(a) and 11(b) present the calculated velocity contours in a stable, non-evaporating liquid rivulet, subject to a cocurrent (figure 2a) and a countercurrent (figure 2b) gas flow, respectively. The velocity contours in figure 11(c) are for a

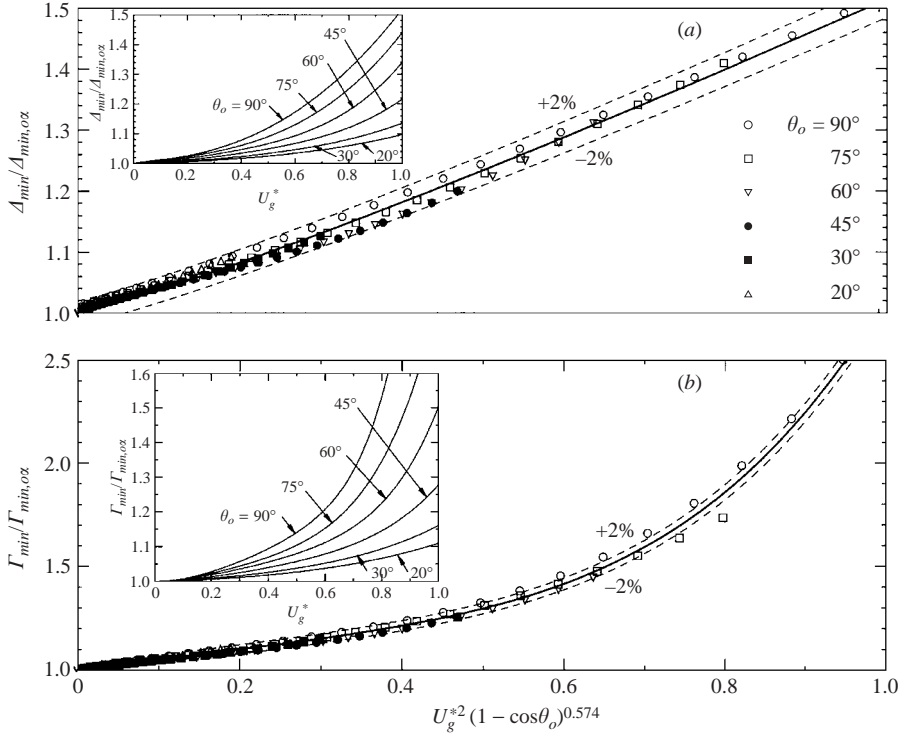


FIGURE 10. Effects of gas velocity and equilibrium contact angle on (a) Δ_{min} and (b) Γ_{min} for a downflowing liquid film, subject to a countercurrent interfacial shear.

climbing liquid rivulet on a vertical surface under the effect of a cocurrent gas flow (figure 2c). The two images in both figures 11(a) and 11(b) are for gas velocities, $U_g^* = 1$ and 2, while the images in figure 11(c) are for gas velocities, $U_g^* = 3$ and 5. All the images in figures 11(a)–11(c) are for $\theta_o = 45^\circ$. The positive and negative dimensionless velocities, U_l^* , indicate downward and upward liquid flows within the rivulet, respectively.

In the rivulets in figure 11(a), the cocurrent interfacial gas velocity, U_g^* , is assisting the gravity, resulting in positive liquid velocities throughout the rivulet (downward). The liquid velocities near the liquid–gas interface increase as the cocurrent gas velocity increases. The highest liquid velocities occur at the rivulet’s plane of symmetry and shift upward toward the liquid–gas interface as the gas velocity increases. Conversely, when the liquid rivulet is subject to a low countercurrent gas flow, the interfacial shear cannot overcome the effect of gravity and the liquid flows downward. However, as the countercurrent gas velocity increases, the interfacial shear overcomes the effect of gravity in the outer region of the rivulet causing the liquid to flow upward (negative velocities), but not in the central region in which the liquid continues to flow downward. Figure 11(b) show that the region in the liquid rivulet that is experiencing the highest downward velocities along the plane of symmetry shifts inward, away from the liquid–gas interface, as the countercurrent interfacial gas velocity increases.

When the dimensional countercurrent gas velocity $U_g^* = 1$, the liquid velocities in the rivulet are positive everywhere, indicating a downward liquid flow. When the countercurrent gas velocity increases to $U_g^* = 2$, the liquid velocities in the rivulet become negative (up flow) everywhere in the region in the middle of the

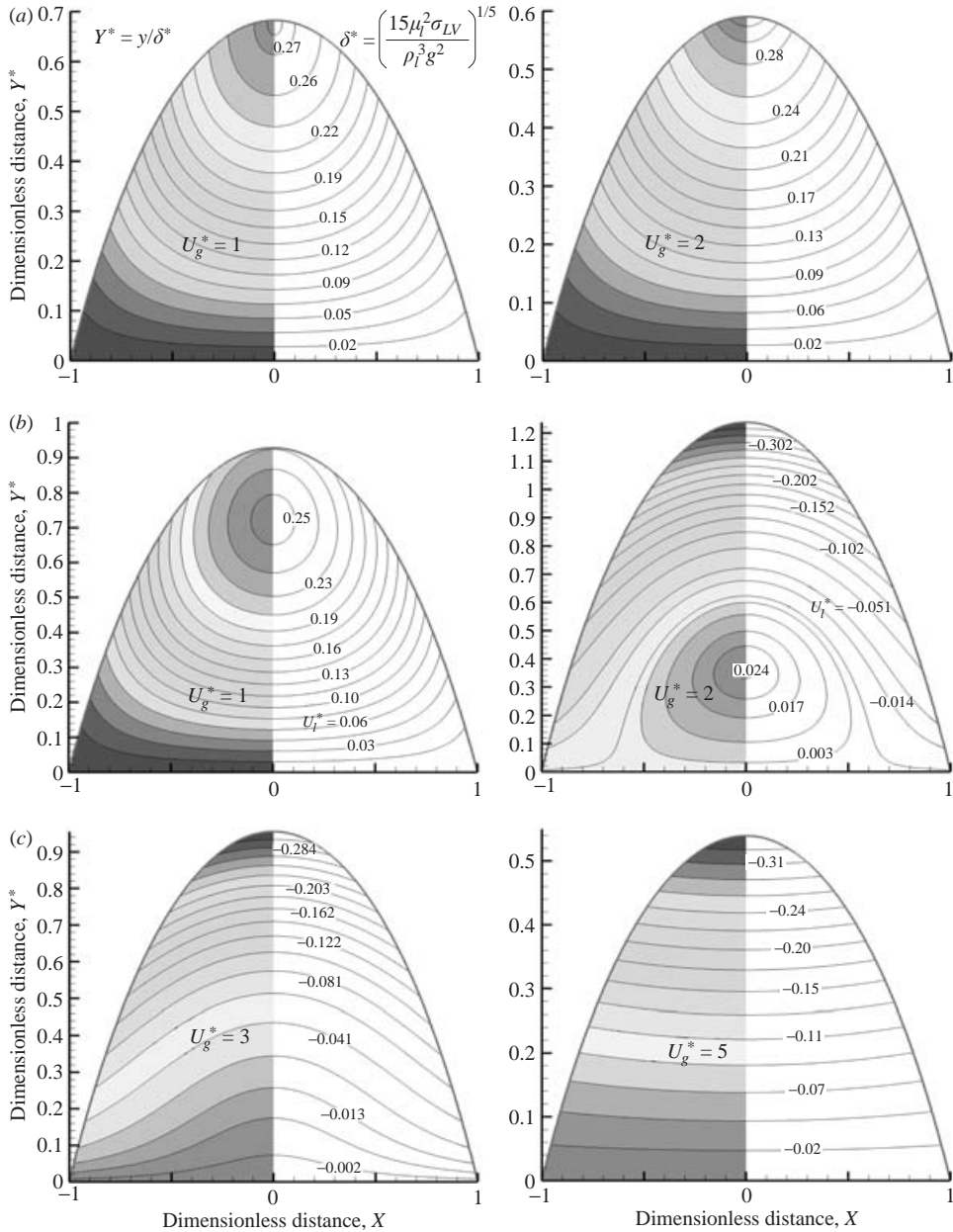


FIGURE 11. Calculated velocity contours in liquid rivulets forming following the breakup of liquid film subject to (a) cocurrent gas flow (figure 2a), (b) countercurrent gas flow (figure 2b), and for (c) a climbing liquid film driven by an upward gas flow (figure 2c). $\theta_o = 45^\circ$.

bottom third of the rivulet. In this region, the liquid velocities are positive (down flow). At such countercurrent gas velocity ($U_g^* = 2$), the net liquid flow in the rivulet is upward, indicating a transition to a climbing liquid film. When the upward gas velocity increases to $U_g^* \geq 3$, the entire liquid flow in the rivulet becomes upward (negative velocities everywhere in the rivulet), indicating a climbing liquid film (figure 11c).

9. Summary

This work investigated the breakup of a non-evaporating liquid film flowing on a vertical or inclined surface and subject to either cocurrent or countercurrent interfacial shear (or gas flow). The three cases considered are: (i) a downflowing liquid film subject to a cocurrent gas flow, (ii) a downflowing liquid film subject to a countercurrent gas flow, and (iii) a climbing liquid film driven by an upward (or cocurrent) gas flow. The results of the latter are successfully compared with the reported measurements for a climbing water film by Hewitt & Lacy (1965). The present analysis is based on the minimization of the total energy of a stable rivulet, forming following the breakup of the liquid film. Analytical expressions for the dimensionless film thickness, Δ_{min} , and the corresponding wetting rate, Γ_{min} , at the film breakup are obtained in terms of the liquid equilibrium contact angle, θ_o , the inclination angle of the underlying surface, α_o , the dimensionless gas velocity, U_g^* , and the liquid physical properties. Incorporated in the total energy of the rivulet are the developed approximate analytical expression of the two-dimensional liquid flow velocity and an analytical expression of the rivulet profile. The two-dimensional liquid velocity distribution in the rivulet, $u_l(x, y)$, is obtained using the Ritz method.

For a liquid film flowing down an inclined surface and subject to a cocurrent gas flow, increasing the gas velocity or decreasing θ_o , decreases both Δ_{min} and Γ_{min} , below their values with zero interfacial shear. Conversely, for a liquid film flowing down an inclined surface and subject to countercurrent (or upward) gas flow, increasing the gas velocity or increasing θ_o , increases both Δ_{min} and Γ_{min} , above their values with zero interfacial shear.

Results show that the liquid flow in the rivulet is downward everywhere as long as the dimensionless countercurrent gas velocity $U_g^* \leq 1$. For $2 < U_g^* < 3$, the net liquid flow as well as the liquid velocities in the rivulet are upward, except at the plane of symmetry near the underlying surface. When $U_g^* \geq 3$, the liquid flow in the rivulet is upward everywhere, which is indicative of a climbing liquid rivulet where the induced traction at the liquid–gas interface overcomes and exceeds the effect of gravity. The developed analytical expression for Γ_{min} is in good agreement with the reported experimental values by Hewitt & Lacy (1965) for a climbing water film on a vertical surface. In these experiments, $U_g^* > 17$ and the measured equilibrium contact angle was $49^\circ \pm 4^\circ$.

This research is funded by the University of New Mexico's Institute for Space and Nuclear Power Studies.

REFERENCES

- ALLEN, R. F. & BIGGIN, C. M. 1974 Longitudinal flow of a lenticular liquid filament down an inclined plane. *Phys. Fluids* **17**, 287.
- ANDROS, F. E. 1980 Heat transfer characteristics of the two-phase closed thermosyphon (wickless heat pipe) including direct flow observation. PhD dissertation, Arizona State University, Tempe, AZ, USA.
- BANKOFF, S. G. 1971 Minimum thickness of a draining liquid film. *Intl J. Heat Mass Transfer* **14**, 2143.
- DONIEC, A. 1991 Laminar flow of a liquid rivulet down a vertical solid surface. *Can. J. Chem. Engng* **69**, 198.
- EL-GENK, M. S. & SABER, H. H. 2001 Minimum thickness of a flowing down liquid film on a vertical surface. *Intl J. Heat Mass Transfer* **44**, 2809.

- EL-GENK, M. S. & SABER, H. H. 2002 An investigation of the breakup of an evaporating liquid film, falling down a vertical uniformly heated wall. *J. Heat Transfer* **124**, 39.
- GROLMES, M. A., LAMBERT, G. A. & FAUSKE, H. K. 1974 Flooding in vertical tubes. *AIChE Symp. Series No. 38, Multiphase Flow Systems*, Paper A4.
- HARTELY, D. E. & MURGATROYD, W. 1964 Criteria for the break-up of thin liquid layers flowing isothermally over solid surface. *Intl J. Heat Mass Transfer* **7**, 1003.
- HEWITT, G. F. & LACEY, P. M. C. 1965 The breakdown of the liquid film in annular two-phase flow. *Intl J. Heat Mass Transfer* **8**, 781.
- HOBLER, T. 1964 Minimum surface wetting (in Polish). *Chemia Stosow.* **2B**, 145.
- KALLIADASIS, S. 2000 Nonlinear instability of a contact line driven by gravity. *J. Fluid Mech.* **413**, 355.
- KING, A. C. & TUCK, E. O. 1993 Thin liquid layers supported by steady air-flow surface traction. *J. Fluid Mech.* **251**, 709.
- LEE, S. C. & BANKOFF, S. G. 1983 Stability of steam–water countercurrent flow in an inclined channel: flooding. *J. Heat Transfer* **105**, 713.
- MIKIELEWICZ, J. & MOSZYNSKI, J. R. 1976 Minimum thickness of a liquid film flowing vertically down a solid surface. *Intl J. Heat Mass Transfer* **19**, 771.
- MUNAKATA, T., WATANABE, K. & MIYASHITA, K. 1975 Minimum wetting rate on wetted–wall column. *J. Chem. Engng Japan* **8**, 440.
- PONTER, B., DAVIES, G. A., ROSS, T. K. & THORNLEY, P. G. 1967 The influence of mass transfer on liquid film breakdown. *Intl J. Heat Mass Transfer* **10**, 349.
- REDDY, J. N. 1984 *An Introduction to the Finite Element Method*. McGraw-Hill.
- WILSON, S. K., DUFFY, B. R. & HUNT, R. 2002 A slender rivulet of a power-law fluid driven by either gravity or a constant shear stress at the free surface. *Q. J. Mech. Appl. Maths* **55**, 385.
- YOUNG, G. W. & DAVIS, S. H. 1987 Rivulet instabilities. *J. Fluid Mech.* **176**, 1.